Ultrafast Dissociation of Metastable CO^{2+} in a Dimer

Xiaoyan Ding,[1] M. Haertelt,[1] S. Schlauderer,[1] M. S. Schuurman,[2,3] A. Yu. Naumov,[1] D. M. Villeneuve,[1] A. R. W. McKellar,[2] P. B. Corkum,[1] and A. Staudte[1]

[1]*Joint Attosecond Science Laboratory, National Research Council and University of Ottawa, Ottawa, Ontario, Canada K1A 0R6*
[2]*National Research Council, 100 Sussex Dr., Ottawa, Ontario, Canada K1A 0R6*
[3]*Department of Chemistry and Biomolecular Sciences, University of Ottawa, 10 Marie Curie, Ottawa, Canada K1N 6N5*

(Received 12 October 2016; revised manuscript received 9 March 2017; published 14 April 2017)

We triply ionize the van der Waals bound carbon monoxide dimer with intense ultrashort pulses and study the breakup channel $(CO)_2^{3+} \rightarrow C^+ + O^+ + CO^+$. The fragments are recorded in a cold target recoil ion momentum spectrometer. We observe a fast CO^{2+} dissociation channel in the dimer, which does not exist for the monomer. We found that a nearby charge breaks the symmetry of a $X^3\Pi$ state of CO^{2+} and induces an avoided crossing that allows a fast dissociation. Calculation on the full dimer complex shows the coupling of different charge states, as predicted from excimer theory, gives rise to electronic state components not present in the monomer, thereby enabling fast dissociation with higher kinetic energy release. These results demonstrate that the electronic structure of molecular cluster complexes can give rise to dynamics that is qualitatively different from that observed in the component monomers.

DOI: 10.1103/PhysRevLett.118.153001

Albeit very weak, van der Waals and electrostatic interactions can have a critical influence on the decay of electronic excitation in a cluster. A prominent example is the interatomic Coulombic decay [1], where electronic excitation is efficiently transferred over a large distance within a dimer [2–4] to allow for a fast nonradiative relaxation.

Here, we show that in a van der Waals complex a different rapid decay mechanism exists, which does not involve the transfer of electronic excitation. Specifically, we use the example of the ultrafast dissociation of metastable CO^{2+} in the triply charged dimer $(CO)_2^{3+}$ and show it is a direct consequence of the weak interactions in the complex.

The monomer CO^{2+} has been extensively investigated as a model system of a metastable molecular dication (e.g., Refs. [5–8] and references therein). The lowest electronic states, the $X^3\Pi$, $a^1\Sigma^+$, and $b^1\Pi$ states, are metastable. The lifetimes of these states range between tens of picoseconds to seconds [5–10]. In the dimer, however, we observe not only the slow dissociation of the CO^{2+}, but also a fast dissociation which is not expected from monomers.

Previous experiments on optical tunnel-ionization of the ArCO complex observed two distinct dissociation channels of the triple-ionization-induced three-body breakup $ArCO \rightarrow Ar^+ + C^+ + O^+ + 3e^-$ [11]. Since the van der Waals interaction is weak, the bond between Ar and the other fragment(s) is broken promptly following ionization. In the sequential breakup channel, the CO^{2+} dissociates at much later time than the initial Ar-CO bond cleavage. Conversely, in the direct channel, the two bonds break simultaneously, resulting in the observation of short lived CO^{2+} species. However, the mechanism behind this rapid dissociation was not discussed.

In our experiment the CO dimer is created in the supersonic expansion of CO at 5 bar through a 10 μm nozzle, cooled to 120 K. Based on our ion mass spectra we estimate that around 5% of all events originate from $(CO)_2$. We record the 3-dimensional momentum of each ion in COLTRIMS [12]. Circularly polarized 800 nm, 25 fs pulses are produced by a Ti:Sapphire laser system (Coherent Legend Elite Cryo) with 10 kHz repetition rate. The laser pulses are focused into the molecular beam with a parabolic mirror to a peak intensity of 6×10^{14} W/cm^2. The laser pulse removes multiple electrons from the dimer and different breakup channels are observed.

We concentrate on the breakup channel $(CO)_2^{3+} \rightarrow C^+ + O^+ + CO^+$. Two-particle breakup channels $(CO)_2^{2+} \rightarrow CO^+ + CO^+$ and $CO^{2+} \rightarrow C^+ + O^+$ are also used for comparison with the three-particle dimer breakup. For all dissociation channels, we select events where the sum momentum of the fragments is low [$|\mathbf{p}_{C^+} + \mathbf{p}_{O^+} + \mathbf{p}_{CO^+}| <$ 10 atomic units (a.u.)] and their relative momentum is high ($|\mathbf{p}_{C^+} - \mathbf{p}_{O^+}| > 50$ a.u. and $|\mathbf{p}_{CO^+}| > 40$ a.u.) to make sure the fragments are correlated, i.e., from the same dimer. All data shown below are for correlated events.

The distribution of CO^+ momentum is shown in Fig. 1(a). The CO^+ momentum has a narrow peak between 100 and 120 a.u. on top of a wide distribution from 40 to 170 a.u. We fit the momentum distribution to the sum of two Gaussian functions, shown as blue and red curves in Fig 1(a). We separate all the events into two subsets: I, the broad peak, $|\mathbf{p}_{CO^+}| < 100$ a.u. or $|\mathbf{p}_{CO^+}| > 120$ a.u.; II, the narrow peak, 100 a.u. $< |\mathbf{p}_{CO^+}| < 120$ a.u.

In Figs. 1(b)–1(d) we plot 2D histograms of the momenta of the fragments in the three-particle breakup channel. We define the direction along the momentum of CO^+, $\mathbf{p}_{CO^+}$, as

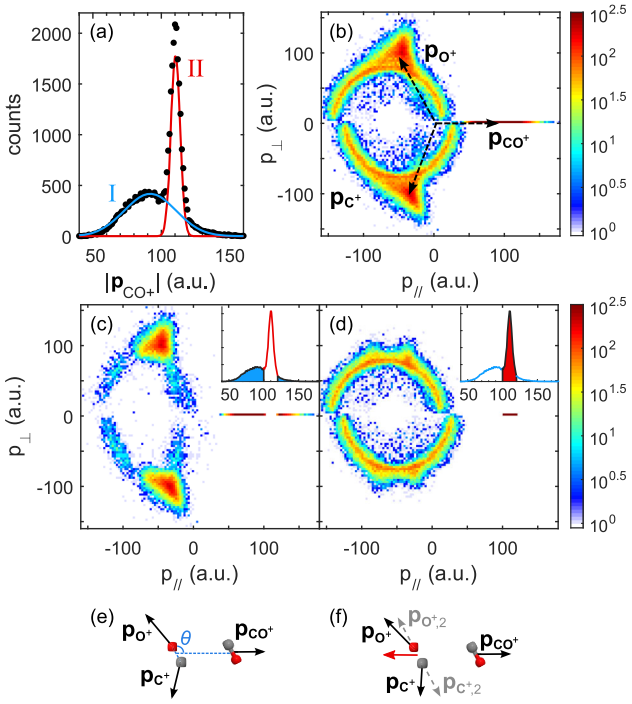

FIG. 1. (a) Momentum distribution of CO^+. Black dots show experimental data; red and blue curves show the fitting with two Gaussian distributions. (b) Newton diagram for all events in the channel $(CO)_2^{3+} \rightarrow C^+ + O^+ + CO^+$. (c)–(d) are Newton diagrams for events in different subsets. Corresponding CO^+ momentum is shown in the top right insets. (c) $|\mathbf{p}_{CO^+}| <$ 100 a.u. or $|\mathbf{p}_{CO^+}| >$ 120 a.u.; (d) 100 a.u. $< |\mathbf{p}_{CO^+}| <$ 120 a.u.. (e) and (f) Sketches of direct and sequential dissociation processes. Black arrows, the final momentum of each fragment; red arrow, momentum of CO^{2+} in the first dissociation step; gray arrows, momentum of C^+ or O^+ from the second dissociation step. Geometry with minimum energy is shown as an example.

$p_\parallel$, and the momentum of O^+, $\mathbf{p}_{O^+}$, as the positive direction of the $p_\perp$ axis. Such a 2D histogram is called a Newton diagram. Figure 1(b) shows the Newton diagram for all correlated events, Figs. 1(c) and 1(d) for the subsets I and II, respectively. These distinct structures in Figs. 1(c) and 1(d) suggest different dissociation processes.

In the following we will establish subset II as a sequential dissociation. There are two steps in the sequential process: first, the dimer breaks into CO^+ and CO^{2+}, and the two fragments propagate under Coulomb interaction; second, the CO^{2+} dissociates into C^+ and O^+. After the first dissociation step, the orientation of the two molecular ion fragments relative to each other becomes random as they propagate. This results in the half-ring structure in the momentum of C^+ and O^+. We compare subset II to two independent two-particle breakups: a CO dimer breakup into two singly charged monomers, $(CO)_2^{2+} \rightarrow CO^+ + CO^+$, and a monomer breakup, $CO^{2+} \rightarrow C^+ + O^+$.

Figure 2(a) shows the kinetic energy of CO^+ from subset II and the two-particle dimer breakup, $(CO)_2^{2+} \rightarrow CO^+ + CO^+$.

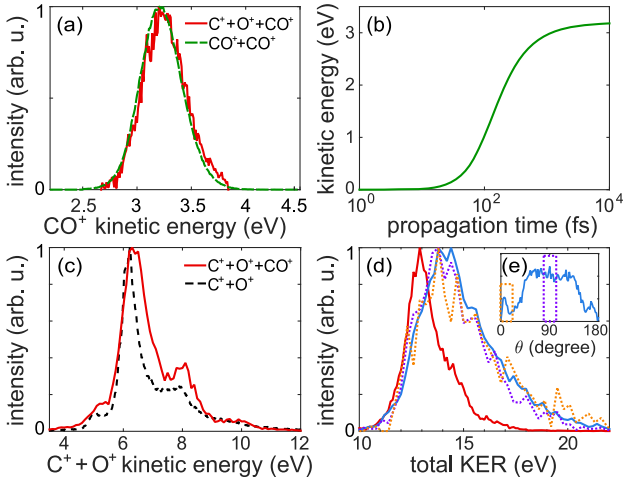

FIG. 2. (a) Kinetic energy distribution of CO^+, solid red curve for the sequential dimer breakup $(CO)_2^{3+} \rightarrow C^+ + O^+ + CO^+$ (subset II) and dashed green curve for the two-particle dimer breakup $(CO)_2^{2+} \rightarrow CO^+ + CO^+$. Kinetic energy for the latter channel is multiplied by 2 to compensate for the charge difference in the two channels. (b) Kinetic energy of CO^+ in the breakup channel $(CO)_2^{3+} \rightarrow CO^{2+} + CO^+$ as a function of propagation time. (c) Kinetic energy of C^+ and O^+, solid red curve for the second step of dimer sequential breakup, dashed black curve for monomer breakup $CO^{2+} \rightarrow C^+ + O^+$. (d) Total kinetic energy release in the three-particle dimer breakup process. Solid blue curve is for subset I, direct breakup channel; solid red curve for subset II, sequential channel. The dotted curves are for specific geometries in the subset I: orange curve for $\theta < 20°$ and purple curve for $80 < \theta < 100°$. (e) Bond angle distribution of the dimer in subset I.

The kinetic energy for the latter channel is multiplied by 2 to compensate for the difference in charge state. Furthermore, we subtracted the background in subset II, assuming a linear contamination from subset I. The kinetic energy distributions for the two channels overlap very well. This confirms that subset II is a sequential process, where CO^{2+} does not dissociate until the CO^+ attains the asymptotic momentum from the two-body Coulomb interaction. By the same argument, we hypothesize that subset I is a direct three-particle breakup.

To estimate the time delay between the two steps in the sequential breakup, we simulate the breakup process $(CO)_2^{3+} \rightarrow CO^{2+} + CO^+$ by solving the kinematic equations, assuming the ions are point particles with charges and masses. Figure 2(b) shows the kinetic energy of CO^+ as a function of propagation time. The simulation shows that it takes about 1 ps to convert the Coulomb potential energy to kinetic energy of the fragments. Therefore, we conclude that the CO^{2+} in the sequential dimer breakup channel has a lifetime longer than 1 ps, and that CO^{2+} in the direct channel dissociates within 1 ps. Since the lifetime of CO^{2+} monomers in low-lying electronic states is at least several picoseconds [10], the direct dissociation only exists in the dimer.

The most straightforward way to study the CO^{2+} breakup in the direct channel would be to compare its kinetic energy release to the monomer breakup. However, in the direct breakup all three fragments interact with each other simultaneously. This means we cannot get the pure kinetic energy release in the C-O bond breaking process. Therefore, we compare the monomer dissociation to the sequential breakup channel, and then compare sequential breakup to the direct breakup channel.

Figure 2(c) plots the kinetic energy release of $C^+ + O^+$ from the monomer breakup and the second step of sequential dimer breakup. In the sequential three-body breakup, the kinetic energy release of the second step is $KE = \frac{1}{2}|\mathbf{p}_{C^+,2}|^2/m_C + \frac{1}{2}|\mathbf{p}_{O^+,2}|^2/m_O$, where $\mathbf{p}_{C^+,2} = \mathbf{p}_{C^+} + \mathbf{p}_{CO^+}(m_C/m_{CO})$ and $\mathbf{p}_{O^+,2} = \mathbf{p}_{O^+} + \mathbf{p}_{CO^+}(m_O/m_{CO})$ are the momenta from the CO^{2+} breakup. The kinetic energy distributions of the two processes are almost identical. Therefore, the CO^{2+} in the sequential dimer breakup channel dissociate from the same electronic states as the monomer CO^{2+}. The peak near 6.2 eV corresponds to dissociation from the $X^3\Pi$, $a^1\Sigma^+$, and $b^1\Pi$ state. The peak around 8 eV is from the $A^3\Sigma^+$ state [6,13,14]. The kinetic energy for the second step of the sequential dimer breakup is about 0.2 eV higher than that for the monomer. This is probably because in the dimer, the first breakup step can excite the CO^{2+} vibrationally and rotationally. When CO^{2+} dissociates, the rovibrational energy becomes translational kinetic energy of C^+ and O^+, resulting in slightly higher kinetic energy release.

Figure 2(d) compares the total kinetic energy release of the fast direct breakup channel (subset I, solid blue curve) to the sequential breakup channel (subset II, solid red curve). The kinetic energy release of the direct channel is about 1.2 eV higher than that of the sequential channel. Figures 2(a) and 2(c) show that the sequential breakup produces fragments in the lowest electronic final states. Hence, the higher kinetic energy release in the direct breakup could be explained by an initial population of higher electronic states in the $(CO)_2^{3+}$ or a dependence on the dimer geometry.

We fit the geometries of the dimers in the direct channels with an iterative algorithm [15], assuming a Coulomb potential between the two CO ions and $^3\Sigma^-$ potential between the C^+ and O^+. We define the angle θ between the C-O covalent bond and the van der Waals bond, as shown in Fig. 1(e). The fitting results reveal that θ has a wide distribution between 0° and 180°; see Fig. 2(e). Thus, the direct channel does not select a specific geometry.

In Fig. 2(d) we plot the kinetic energy release of the dimers with bond angle $\theta < 20°$ (dotted orange curve) and $80 < \theta < 100°$ (dotted purple curve). The dimers with different bond angles have a similar kinetic energy release. This rules out the possibility that different geometries cause the difference in kinetic energy release of the fast and slow channels.

To investigate the origin of the dimer-specific fast dissociation channel, we compute potential energy curves for the $(CO)_2^{3+}$ dimer complex using *ab initio* electronic structure methods. We compute these curves using two different approaches. The first assumes that CO^+ is simply a point charge, resulting in perturbed CO^{2+} dissociation curves. The second approach explicitly considers the electronic structure of the CO^+ and computes the potential energy surfaces of the total dimer complex. The calculations were performed employing multireference complete active space (CASSCF) wave functions in conjunction with a multireference configuration interaction (MRCI) treatment of dynamical electron correlation [16,17].

Figure 3(a) illustrates the relevant molecular orbitals and potential energy curves. HOMO-1 and HOMO orbitals of CO are the (fully occupied) 1π and 5σ, respectively. The $X^3\Pi$ state of CO^{2+} arises from a $1\pi^3 5\sigma^1$ electronic

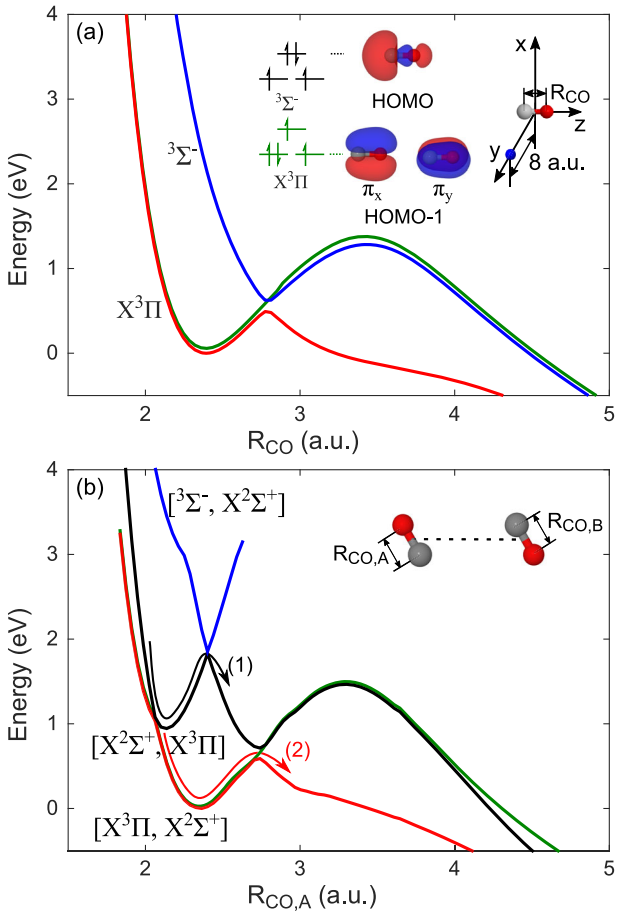

FIG. 3. (a) Potential energy curves of CO^{2+} with a point charge. The Coulomb field of the point charge perturbs the π_x and π_y orbitals differently, which breaks the symmetry of one $X^3\Pi$ electronic state. An avoided crossing arises between one component of the $X^3\Pi$ states and the $^3\Sigma^-$ state. (b) *Ab initio* potential energy curves of the CO^+-CO^{2+} complex. Arrows show possible dissociation pathways. Kinetic energy release from pathway (1) is 1.2 eV higher than from pathway (2).

configuration and the $^3\Sigma^-$ state arises from a $1\pi^2 5\sigma^2$ electronic configuration. When the dication is in an electric field free environment, molecular symmetry precludes any nonadiabatic coupling between these states. However, a positive charge at a distance of 8 a.u. (the ground state intermolecular distance [18,19]), as illustrated in the top right inset in Fig. 3(a), differentially distorts the π_x and π_y orbitals. This breaks the symmetry of the $^3\Pi$ state, and thereby engenders an avoided crossing between one component of the $X^3\Pi$ and the $^3\Sigma^-$ state.

The next two lowest-lying electronic states, $a^1\Sigma^+$ and $b^1\Pi$, are singlet states. For both the monomer and dimer, these states can only couple to the $^3\Sigma^-$ state via spin-orbit interaction. The coupling between these states has been investigated previously in the monomer [9], and is of a magnitude insufficient to account for the short lifetimes required to lead to rapid dissociation. Therefore, we do not consider these states in the following discussion of the direct dissociation channel.

Thus, in contrast to the CO^{2+} monomers, which can only dissociate via spin-orbit coupling, the CO^{2+} in the dimer has a direct adiabatic dissociation channel via the avoided crossing between the $X^3\Pi$ and $^3\Sigma^-$ states. However, the charge-induced avoided crossing does not explain why the kinetic energy release for the fast pathway is higher than that observed for the "slow" channel.

The assumption that the CO^+ counterion can be represented as a point charge (thereby neglecting its electronic structure) is tested by computing the dissociation curves of a component CO in the $(CO)_2^{3+}$ complex. As Fig. 3(b) illustrates, we observe a new low-lying electronic state for the dimer system, a component of the degenerate ground state of the dimer, not present in the point charge model. This new electronic state arises from the fact that the different charge states can be located on either one of the constituent CO monomers. Specifically, the dicationic species may localize on either of the two component CO moieties. When the two CO bond lengths are identical, these CO molecules are indistinguishable and the solutions are degenerate, resulting in the curve crossing in Fig. 3(b) at $R_{CO,A} \sim 2.1$ a.u. The coupling of states on each component monomer gives rise to a new manifold of electronic states which can be determined from excimer theory [20]. This new excited state of the dimer crosses the dissociative $^3\Sigma^-$ state 1.2 eV above the lower crossing with the ground state. This value is consistent with the observed difference in kinetic energy release of the two channels. Thus, we conclude that the electronic structure of the CO^+ counterion has a non-negligible influence on the decay dynamics of the triply charged complex.

This picture is fully consistent with previous ArCO results. In particular, computations show that the electronic structure of the Ar atom leads to new dissociation channels in the complex via the coupling of CO^{2+}-Ar^+ and CO^+-Ar^{2+} charge states. The same mechanisms discussed in the present Letter can be applied to these previous studies, where the only differences are quantitative and arise from different relative electronic state energies since the ionization potentials of the CO and Ar moieties are distinct [i.e., in $(CO)_2^{3+}$ they are identical].

In conclusion, our results suggest that a new CO^{2+} dissociation channel emerges when it is placed in a van der Waals complex with a cationic counterion. This new channel differs from the monomer channel in two key ways: (1) it occurs on a shorter time scale than the nascent monomer channel, and (2) it is associated with a larger kinetic energy release. The computed potential curves suggest a straightforward explanation for the first point. The symmetry breaking induced by the counter charge leads to an avoided crossing and adiabatic dissociation channel, whereas the monomer dissociates only via the (weaker) spin-orbit coupling. The second observation, that the new channels result in higher kinetic energy release, is potentially explained by the presence of a low-lying excited state of the dimer that arises due to coupling of charge states on the two component CO moieties. However, the initial wave packet prepared by the ionizing field cannot be well characterized by the present experiment. Thus, conclusive evidence for ionizing to an excited state of the dimer remains to be shown. However, such a channel would be expected to produce CO^+ fragments with significantly lower internal energy than those produced via a ground electronic state process. This difference provides a potential experimental method for validating the current model.

M. H. acknowledges a Feodor-Lynen fellowship from the Alexander von Humboldt Foundation. We thank A. Avery and D. Crane for technical support. We are also indebted to Ph. Bunker, U. Thumm, and M. Spanner for helpful discussions. Financial support from the National Science and Engineering Research Council Discovery Grants No. 419092-2013-RGPIN and No. 2015-06730-RGPIN, the DAAD rise program, Canada Foundation for Innovation, and the Ontario Research Fund is gratefully acknowledged.

[1] L. S. Cederbaum, J. Zobeley, and F. Tarantelli, Phys. Rev. Lett. **79**, 4778 (1997).
[2] U. Frühling, F. Trinter, F. Karimi, J. Williams, and T. Jahnke, J. Electron Spectrosc. Relat. Phenom. **204**, 237 (2015).
[3] T. Jahnke, H. Sann, T. Havermeier, K. Kreidi, C. Stuck, M. Meckel, M. Schöffler, N. Neumann, R.Wallauer, S. Voss, A. Czasch, O. Jagutzki, A. Malakzadeh, F. Afaneh, T. Weber, H. Schmidt-Böcking, and R. Dörner, Nat. Phys. **6**, 139 (2010).
[4] F. Trinter, M. S. Schöffler, H.-K. Kim, F. P. Sturm, K. Cole, N. Neumann, A. Vredenborg, J. Williams, I. Bocharova, R. Guillemin, M. Simon, A. Belkacem, A. L. Landers,

T. Weber, H. Schmidt-Böcking, R. Dörner, and T. Jahnke, Nature (London) **505**, 664 (2014).
[5] L. H. Andersen, J. H. Posthumus, O. Vahtras, H. Agren, N. Elander, A. Nunez, A. Scrinzi, M. Natiello, and M. Larsson, Phys. Rev. Lett. **71**, 1812 (1993).
[6] M. Lundqvist, P. Baltzer, D. Edvardsson, L. Karlsson, and B. Wannberg, Phys. Rev. Lett. **75**, 1058 (1995).
[7] M. Hochlaf, R. I. Hall, F. Penent, H. Kjeldsen, P. Lablanquie, M. Lavollée, and J. H. D. Eland, Chem. Phys. **207**, 159 (1996).
[8] J. P. Bouhnik, I. Gertner, B. Rosner, Z. Amitay, O. Heber, D. Zajfman, E. Y. Sidky, and I. Ben-Itzhak, Phys. Rev. A **63**, 032509 (2001).
[9] T. Šedivcová, P. R. Ždánská, and V. Špirko, J. Chem. Phys. **124**, 214303 (2006).
[10] F. Mrugala, J. Chem. Phys. **129**, 064314 (2008).
[11] X. Gong, M. Kunitski, L. P. H. Schmidt, T. Jahnke, A. Czasch, R. Dörner, and J. Wu, Phys. Rev. A **88**, 013422 (2013).
[12] J. Ullrich, R. Moshammer, A. Dorn, R. Dörner, L. P. H. Schmidt, and H. Schmidt-Böcking, Rep. Prog. Phys. **66**, 1463 (2003).
[13] S. De *et al.*, Phys. Rev. A **84**, 043410 (2011).
[14] F. Penent, R. I. Hall, R. Panajotović, J. H. D. Eland, G. Chaplier, and P. Lablanquie, Phys. Rev. Lett. **81**, 3619 (1998).
[15] F. Légaré, K. F. Lee, I. V. Litvinyuk, P. W. Dooley, S. S. Wesolowski, P. R. Bunker, P. Dombi, F. Krausz, A. D. Bandrauk, D. M. Villeneuve, and P. B. Corkum, Phys. Rev. A **71**, 013415 (2005).
[16] H. Lischka, R. Shepard, R. M. Pitzer, I. Shavitt, M. Dallos, T. Müller, P. G. Szalay, M. Seth, G. S. Kedziora, S. Yabushita, and Z. Zhang, Phys. Chem. Chem. Phys. **3**, 664 (2001).
[17] H. Lischka *et al.*, Columbus, an *ab initio* electronic structure program, release 7.0, 2012.
[18] R. Dawes, X.-G. Wang, and T. Carrington, J. Phys. Chem. A **117**, 7612 (2013).
[19] M. Rezaei, S. Sheybani-Deloui, N. Moazzen-Ahmadi, K. H. Michaelian, and A. R. W. McKellar, J. Phys. Chem. A **117**, 9612 (2013).
[20] S. Levchenko, H. Reisler, A. I. Krylov, O. Gessner, A. Stolow, H. Shi, and A. L. L. East, J. Chem. Phys. **125**, 084301 (2006).